Materials Science & Engineering A 845 (2022) 143199

Contents lists available at ScienceDirect

Materials Science & Engineering A

journal homepage: www.elsevier.com/locate/msea

Role of thermally-stable deformation twins on the high-temperature mechanical response of an austenitic stainless steel

Taymaz Jozaghi [a], Peyman Samimi [b], Yuriy Chumlyakov [c], Ibrahim Karaman [a,b,*]

[a] Department of Mechanical Engineering, Texas A & M University, College Station, TX, 77843, USA
[b] Department of Materials Science and Engineering, Texas A & M University, College Station, TX, 77843, USA
[c] Siberian Physical Technical Institute, Tomsk State University, Tomsk, 634050, Russia

ARTICLE INFO

Keywords:
Austenitic stainless steels
Deformation twins
High temperature properties
Microstructure
Thermal stability

ABSTRACT

In the present study, a two-step thermo-mechanical processing consisting of cold work and heat treatment steps was performed to increase the operating temperature of 316 austenitic stainless steels. A hierarchical microstructure of thermally-stable, nano twin bands was achieved forming into bundles in elongated grains. The mechanical response of the samples with this microstructure was evaluated through uniaxial tension tests at temperatures ranging from 20 °C to 500 °C and compared with those from the fully annealed samples. The results demonstrate that such hierarchical microstructure leads to a significant increase in the elevated temperature yield strengths due to the presence of nano-twin boundaries and resulting decrease in dislocation mean free path and increase in dislocation storage capacity. In fact, the yield strength ratio of the twinned and annealed samples increases with increasing temperature up to 500 °C, indicating the effectiveness of pre-existing thermally-stable twin boundaries as the strengthening source at temperatures as high as 0.46 homologous temperature. The hierarchical microstructure also led to irregular serrations through dynamic strain aging in the stress-strain response at 500 °C, which is attributed to the bi-modal microstructural length-scales present in the structure affecting the diffusion distances during dynamic strain aging. This structure also increases the tensile strength, and without a total loss in ductility, even though the flow stress of the twinned samples surpasses the tensile strength of the annealed samples, especially at elevated temperatures. Total hardening rate is consistently higher in the twinned samples as compared to the annealed samples, indicating the positive role of nano-twin boundaries in the dislocation storage capacity at elevated temperatures. Overall, the present study clearly demonstrate the positive role of thermally stable nano-twins on the elevated temperature mechanical response of austenitic stainless steels.

1. Introduction

With an ultimate motive to increase the operating temperatures of metallic alloys in service to decrease the CO_2 emission [1,2], austenitic stainless steels are considered as a good cost-efficient option due to their high-temperature performance, i.e. oxidation resistance and creep [3–5]. One method to increase the strength of these steels is creating barriers to dislocation motion through thermo-mechanical processing, in order to reduce their mean free path, which can lead to high tensile strength and work hardening exponent [6,7]. One such barrier against dislocation motion can be a twin boundary, created through mechanical processing or recrystallization. In face-centered cubic (fcc) materials, dislocations can have several distinct interactions with twin boundaries: slip (fully or partially) across twin boundary after pile up, glide in twin or matrix lamellae, or glide of partials parallel to twin boundaries. In addition, dislocation may be absorbed by the twin boundary, or may cause de-twinning of the twin boundary [8–10]. Increase in local stress levels due to pile up of dislocations can also lead to activation of secondary twinning systems [9] The dominant mode of interaction mostly depends on the orientation between twin bands and the loading direction, and dislocation density [8,9]. Twin boundaries are also desired at high temperatures because they are low-energy, high-angle coincidence site lattice boundaries [11]. Since they are high-angle boundaries, they can impede dislocation motion and strengthen the alloy, while they are also more stable at higher temperatures as compared to other high angle boundaries due to their lower energy. For example, in nanostructured

* Corresponding author.Department of Mechanical Engineering, Texas A & M University, College Station, TX, 77843, USA.
E-mail address: ikaraman@tamu.edu (I. Karaman).

https://doi.org/10.1016/j.msea.2022.143199
Received 8 January 2022; Received in revised form 19 April 2022; Accepted 22 April 2022
Available online 26 April 2022

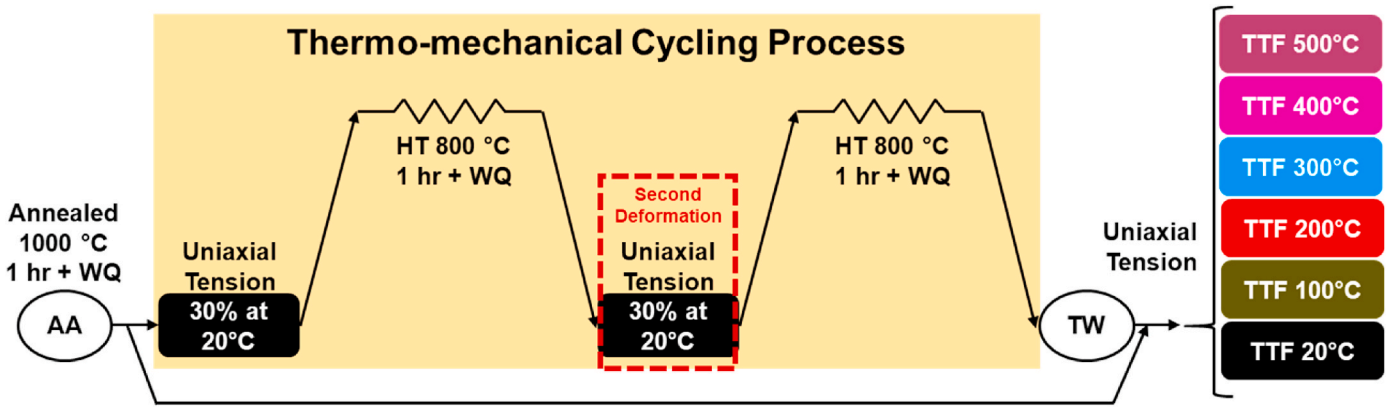

Fig. 1. Schematic of the thermomechanical processing steps to increase the volume fraction of the deformation steels in 316 austenitic stainless steels: several as-annealed (AA) samples went through a thermo-mechanical cycling process to create twinned structured (TW) samples. Both the AA and TW samples were tested in uniaxial tension test to-failure (TTF) at different temperatures. The second deformation of 30% at 20 °C has been pointed out.

316LVM austenitic stainless steel, it was discovered that nano-twin and low-angle boundaries have lower mobility during annealing under hydrostatic pressure, compared to non-equilibrium high-angle grain boundaries [12]. Therefore, the purpose of the present work is to investigate whether these low-energy, high-angle boundaries are effective at strengthening austenitic stainless steels, that exhibit extensive twin formation, at elevated temperatures, and how these pre-existing boundaries affect the ductility.

Twin formation depends on the stacking fault energy (SFE) of the materials and their thickness depends on the lattice friction and other barriers in the lattice [13–15]. In austenitic stainless steels, SFE commonly ranges from low to medium values. Experimental values from literature range from 8 mJ/m^2 to 80 mJ/m^2 for some of the most common austenitic stainless steels [16–20]. In these steels, plastic deformation usually initiates with dislocation slip, then stacking faults are formed due to the separation of dislocation partials, then deformation twinning starts to contribute to the plastic deformation [21]. Deformation twins formed in 316L austenitic stainless steel, for example, play a significant role in increasing the strength and toughness, especially after recovery/recrystallization heat treatments [22].

It is generally known that ductility decreases as strength increases, and that this loss of ductility can be reversed to some extent through recovery and recrystallization of the deformed metals. The reports on the role of twin boundaries on the strength and ductility of materials that twins, however, show potential for a more promising combination of strength and ductility than those in materials that do not twin. Lu et al. [23] have mentioned that existence of three characteristics in a strength-inducing feature can lead to optimization of strength and ductility: coherency with the matrix, thermal and mechanical stability, and sizes smaller than 100 nm. Bouaziz et al. [24] discovered that a higher combination of strength-ductility can be achieved through recovery rather than recrystallization in nano-twinned stainless steels. Simultaneously increasing the strength and ductility in pure copper has been attributed to nano-sized twins [25,26]. In austenitic stainless steels, thermally stable deformation twins formed during one cycle of deformation and annealing can lead to a nano-sized structure with high strength and without a detrimental effect on strain hardening [27]. In 316L austenitic stainless steel, deformation twins, grain refinement, and strain-induced martensite led to strengthening accompanied with decent tensile ductility, which was attributed to the co-existence of slightly-deformed grains with fine, twinned structure [28]. Since dislocations can glide along a coherent twin boundary, smaller twin thicknesses may lead to higher ductility [23]. In another study on 316L austenitic stainless steel, a heterogeneous lamellar structure consisting of nano-sized twin bundles and ultrafine grains resulted in a good combination of ductility and strength: good ductility originating from the deformation of the coarse regions of the structure, and the strength arising from fine grain/twin size [29].

If deformation twins are to impart additional strength at high temperatures, they need to be thermally stable, and persist after a recovery heat treatment. In copper thin films, nano twin bands grew when annealed up to 800 °C (0.74 T_m), but significantly slower than regular grain sizes increased. These thermally stable twin bands contributed to materials strength significantly, maintaining it even though average grain size increased due to annealing [30]. Through differential scanning calorimetry of high-pressure torsion deformed nano-crystalline 316L stainless steel, El-Tahawy et al. found that the dislocations are recovered between ~320 °C and ~470 °C without affecting the average grain size or the phase composition, and α′-martensite is reversed into austenite at ~470 °C–~680 °C [31]. Deformation twins in austenitic Fe–Mn–C steels have been shown to be stable after 1-h heat treatment at 550 °C [32]. In high-Mn twinning-induced plasticity (TWIP) steels, deformation nano-twins were stable up to recrystallization at 625 °C [33]. In another study, nano-twins were found to strengthen a TWIP steel up to 615 °C, where recrystallization happens and strengthening is lost [34]. The coherent nano-twins in deposited 330 austenitic stainless steel were stable up to 500 °C [35]. In a study on 316L austenitic stainless steel, the samples were cold-rolled and heat treated at 750 °C for different durations to create a structure of nano-grains and nano-twins surrounded by lamellar coarse grains and recrystallized grains, and an optimal combination of ~1 GPa yield strength and 20% failure to elongation was achieved. Byun et al. [36] have studied the mechanical response of different conventional austenitic stainless steels, both in annealed and cold worked conditions, at different temperatures in uniaxial tension, and found that strength and uniform strain decrease with increasing temperature. In addition, they found out that the hardening rate and true stress are almost equal at the onset of plastic instability, called this value the plastic instability stress (PIS), and claimed that if the yield strength of cold-worked samples surpassed this PIS of the annealed material, necking occurs right after yielding. More recently, in iron-based superalloys, nano-twins that were formed during dynamic plastic deformation process and survived annealing at 700 °C, were found to both strengthen the material as well as improve the ductility after the annealing. The coexistence of nano-twins with γ′ nano-precipitates led to better mechanical response [37]. The twin-enhanced strengthening was claimed to be due to the thermal and structural stability of nano-twins during precipitation [37].

While the mechanical response of austenitic stainless steels at high temperatures, with different types of structures (combinations of annealed coarse grains, nano grains, nano twin bands, etc.) has been extensively studied, to the best of the author's knowledge, the isolated effect of thermally-stable deformation twins on their mechanical

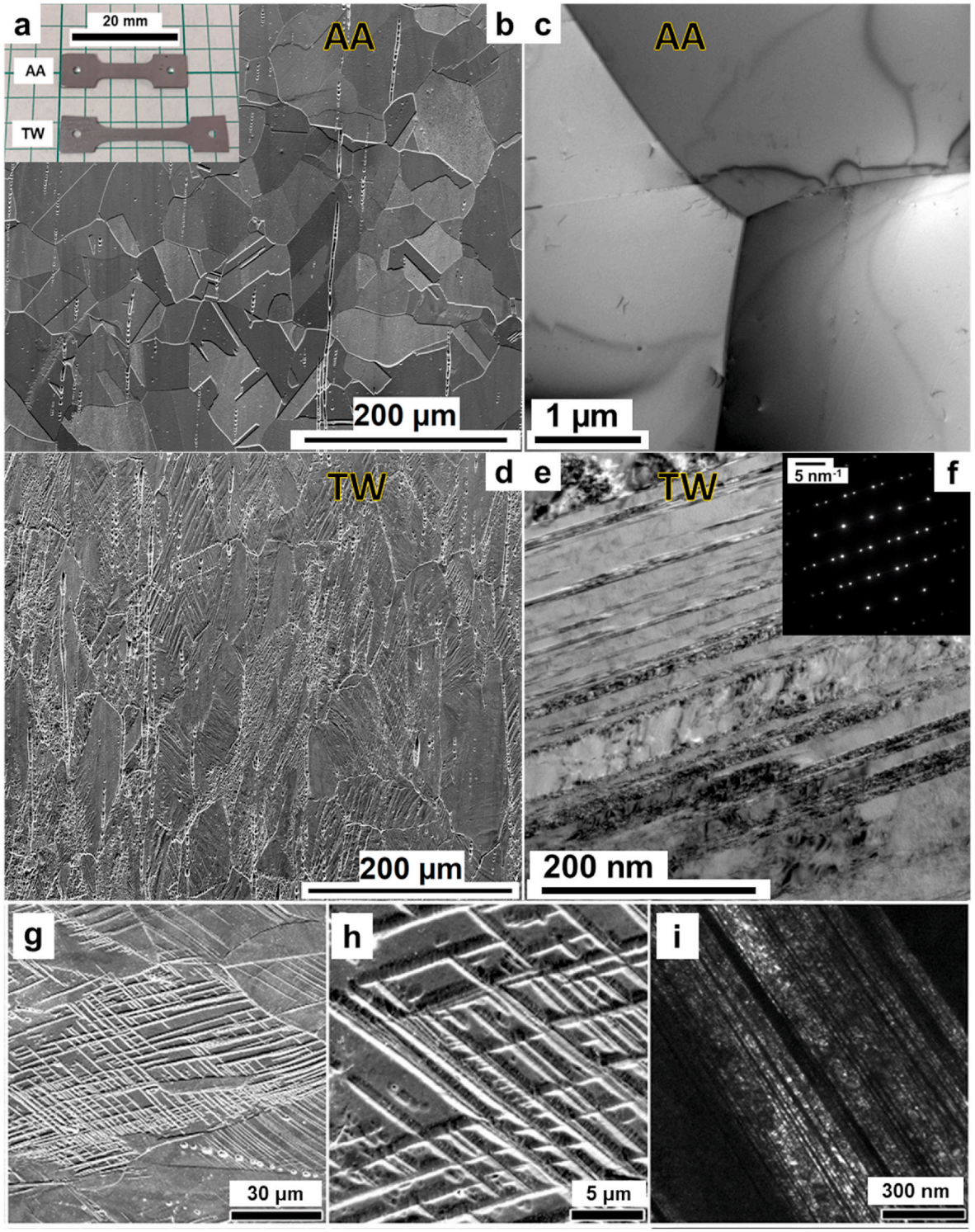

Fig. 2. a) Tensile test specimens of the AA and TW samples of 316 austenitic stainless steel, b) Secondary electron (SE) image of the AA samples, showing equiaxed grains and voids from impurities, c) Bright field TEM image of the AA samples displaying low dislocation density, d) SE image of the TW samples featuring elongated grains, twins and voids, e) TEM image of the TW samples indicating the presence of twin bands, f) Selected area diffraction pattern of the image in (d) confirming {111} <112> twinning. Figures (g) through (i) are from our previous work [38] depicting the presence of the hierarchical structure under one step tensile deformation up to 40% strain.

strength has not been systematically investigated. In our recent study on 316 austenitic stainless steel [38], we demonstrated that deformation twin bundles of ~0.5 µm wide, composed of 30 nm twin bands, are stable up to 900 °C. Then, through cyclic deformation-heat treatments, we increased the volume fraction of these thermally stable deformation twins in the material. The thermally stable, highly-twinned structure was found to strengthen the steel without notable loss of ductility [38]. In the present work, we investigate the mechanical response of such a highly twinned samples at elevated temperatures, for a better understanding of the role of thermally-stable deformation twins on their high temperature mechanical response.

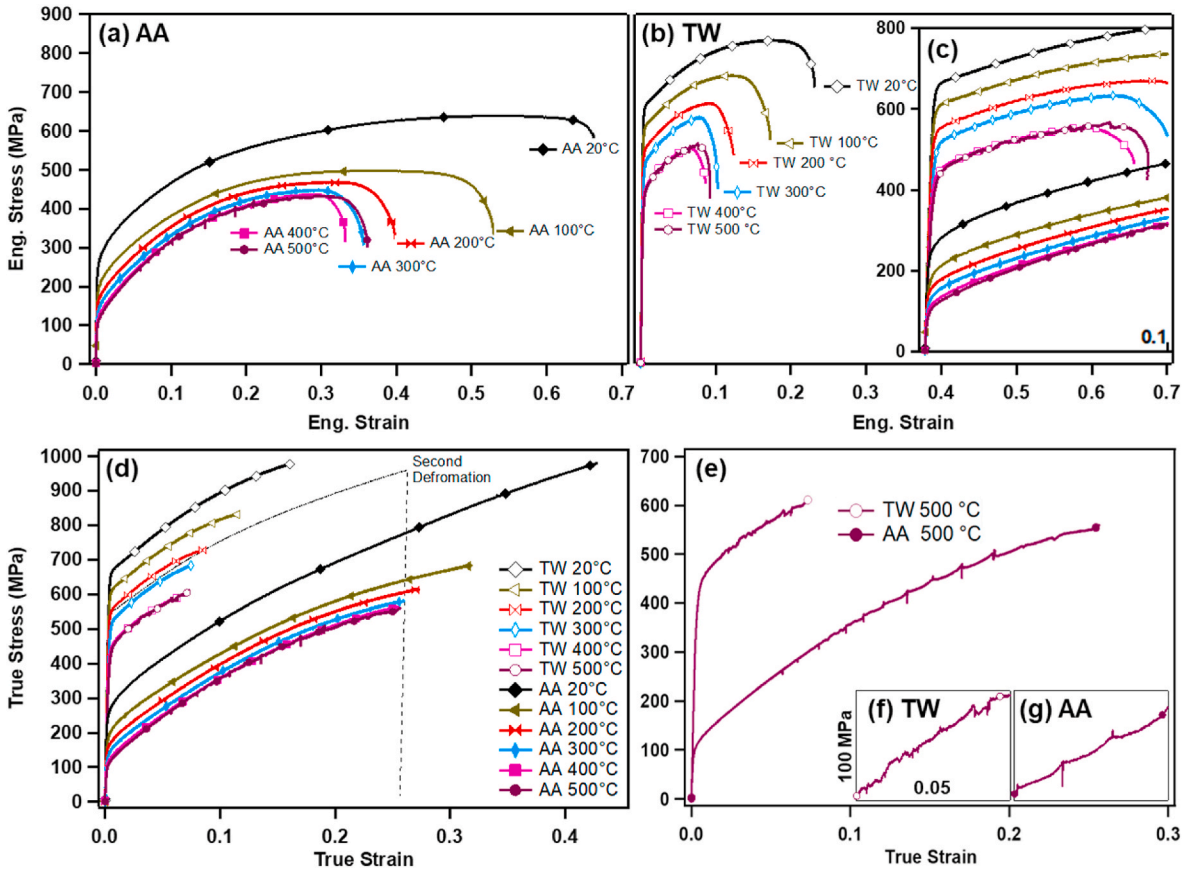

Fig. 3. Stress vs. strain graphs of the uniaxial tension tests for 316 austenitic stainless steel at temperatures from 20 °C to 500 °C. a) Engineering stress vs. engineering strain responses of the AA samples, b) Engineering stress vs. engineering strain responses of the TW samples, c) Engineering stress vs. engineering strain responses of both AA and TW samples in a smaller scale comparing the yield strength levels, d) True stress vs. true strain responses of both AA and TW samples, as well as the second deformation step as depicted in Fig. 1, e) True stress vs. true strain responses of both AA and TW samples at 500 °C, with higher magnification shown in f) and g) for the TW and AA samples, respectively.

2. Experimental procedures

The material in this study is a commercial 316 austenitic stainless steel, acquired in the form of hot-forged billets. Dog-bone shaped tensile specimens were cut from these billets with the gage dimensions of 8 mm × 3 mm × 1 mm using wire electro-discharge machining. The samples were then heat treated (HT) at 1000 °C for 1 h, followed by water quenching (WQ), to prepare **as-annealed (AA)** samples. As presented in the schematic graph in Fig. 1, some of the AA samples went through a thermo-mechanical cycling process that consists of two cycles of 30% deformation at room temperature in uniaxial tension, followed by a heat treatment at 800 °C for 1 h and water quenching in each cycle. This specific process has been designed to increase the volume fraction of deformation twins in the steel, while decreasing the dislocation density through recovery [38]. Sample dimensions and preparations were kept consistent with this previously-established process. Samples, after this thermo-mechanical process, are highly twinned and will be referred to as **twinned (TW)** condition. These TW samples, alongside samples from AA, were then tested in uniaxial tension test until fracture (TTF) at different temperatures. Uniaxial tensile tests were performed on an MTS servo-hydraulic mechanical test frame, with an initial strain rate of 10^{-3} s^{-1}. The temperature was controlled though conduction from heating and cooling the grips; heating by resistive heating-bands, and cooling by passing liquid nitrogen through copper tubing. In order to create a more stabilized atmosphere and temperature, the entire grip and samples were isolated from the environment with a chamber. The temperature was monitored through thermocouples attached to each grip as well as the center of the tensile samples. The strain measured using a high temperature extensometer directly attached to the gage section of the samples. Each tension test condition was repeated at least 3 times, the median graph was selected to be presented in this work, and values were averaged and reported with the corresponding standard deviations.

Microscopy samples were prepared following the standard metallographic sample preparation procedures and then etched using a solution of 10 ml nitric acid, 30 ml hydrochloric acid and 30 ml distilled water for 2–3 min. Scanning Electron Microscope (SEM) images were obtained using a field emission FEI Quanta 600 microscope. Transmission Electron Microscopy (TEM) characterizations were performed using FEI Tecnai G2 F20 microscope operated at 200 kV. The disc specimens for TEM observation were mechanically thinned to <50 μm, and then were prepared using a double-jet electrolytic polishing in a mixture of 10% perchloric acid and 90% ethanol at 20 V and a temperature of almost −20 °C.

3. Results and discussion

Fig. 2 displays the physical samples and the microstructure of the **AA (as-annealed)** and **TW (twinned)** samples before the tensile tests. Fig. 2a shows tensile specimens. The TW samples are longer and thinner than the AA samples since it has undergone the thermo-mechanical process presented in Fig. 1. Fig. 2b is the secondary electron image of an etched AA sample, showing an equiaxed fully-austenitic microstructure with a grain size about 70 μm, a few annealing twins, and voids that were created during etching when the impurities leave the surface. These impurities are aligned perpendicular to the forging orientation of the initial billets. Fig. 2c is the TEM image of the same sample displaying

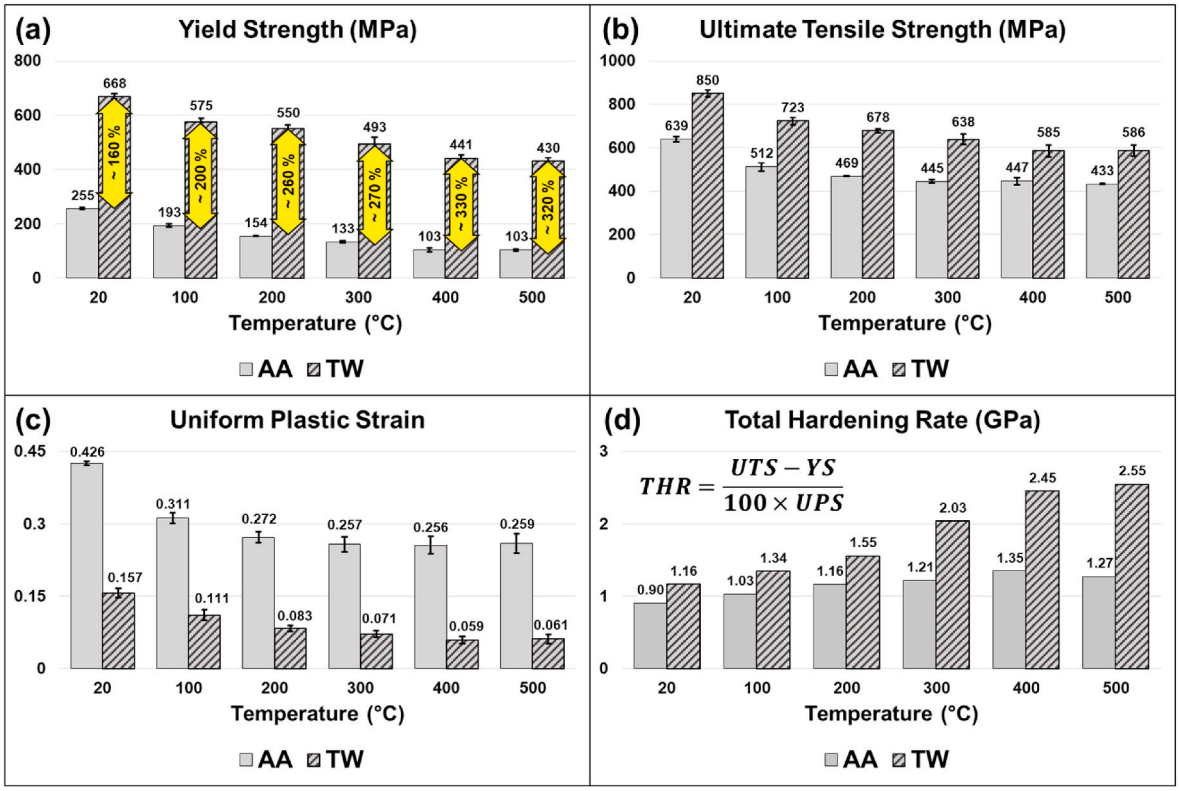

Fig. 4. Summary of the mechanical properties of 316 austenitic stainless steel determined at different temperatures in two different microstructural condition: a) Yield strength (YS) values for the AA and TW samples at different temperatures, and yellow arrows indicating the relative increase in yield strength (defined as the difference between the YS values of the AA and TW samples divided by YS of the AA samples at each temperature), as a result of the thermo-mechanical processing to increase the density of deformation twin boundaries, b) Ultimate tensile strength at different temperatures, c) Uniform plastic strain at different temperatures defined as the true strain after yielding and before necking, and d) Total hardening rate defined as the increase in strength from YS to UTS divided by the uniform plastic strain. (For interpretation of the references to colour in this figure legend, the reader is referred to the Web version of this article.)

a triple junction of grain boundaries and low dislocation density. Fig. 2d is the secondary electron image of an etched TW sample, showing highly elongated grains in the tension direction compared to the AA samples, voids from etched impurities similar to the AA samples, and a high-volume fraction of surface features that are twin bands [38]. From a statistical analysis, it was found that almost all grains show these features, and the total volume fraction of twins in the TW samples is about 30% (while the AA sample after 40% uniaxial tension test features less than 20% volume fraction of twins, Fig. 2g through 2i, [38]). Fig. 2 is the TEM image of the TW samples, showing a high-magnification image of these features, and Fig. 2f is the selected area diffraction pattern, confirming {111} <112> type deformation twins.

Uniaxial tension tests are performed on these two conditions at different temperatures and the results are presented in Fig. 3. Fig. 3a presents the engineering stress (S) vs. engineering strain (e) responses of the AA samples. Similarly, Fig. 3b is the engineering stress (in MPa) vs. engineering strain responses of the TW samples. Both figures are drawn to the same scale, for comparison. These graphs are also presented in Fig. 3c in a smaller scale, up to 800 MPa stress and 10% strain, to better compare the responses of the two different conditions. The yield strength (YS) and ultimate tensile strength (UTS) values from these tests are reported in Fig. 4a and b, respectively. As expected, the strength decreases with increasing temperature. The curve for 500 °C overlaps that of 400 °C almost perfectly, up to necking. The thermo-mechanical processing in Fig. 1 has caused a shift in the stress-strain response upward in the TW samples compared to the AA samples. However, strengthening has occurred with a decrease in ductility. The curve at 500 °C for the TW sample also overlaps that of 400 °C, similar to the AA sample, signifying that the governing physical mechanism causing this temperature invariant response at these two temperatures is not affected by the extra plastic energy stored and microstructural differences in the TW samples as compared to the AA samples.

As the values provided in Fig. 4a demonstrate, yield strength decreases with increasing temperature. Overall, the yield strength of the AA samples decreases from ~250 MPa to ~100 MPa (60% decrease) and for the TW samples, from ~670 MPa to ~430 MPa (~35% decrease) as the temperature is increased from 20 °C to 500 °C. Flow stress in polycrystalline aggregates can be represented using the following equation (Eq. (1)) [39–41]:

$$\sigma = \overline{M}.\alpha.\mu.b.\lambda^{-m} \tag{1}$$

where σ is the flow stress, $\overline{M}$ is the average Taylor factor (representing crystallographic texture), α, μ, and b are a constant, shear modulus, and Burgers vector, respectively, and λ is dislocation mean free path powered to an exponent m. The dislocation mean free path is usually defined based on the effective grain size (d), a constant K, and dislocation density (ρ), as shown in Eq. (2) [38,42]:

$$\frac{1}{\lambda} = \frac{1}{d} + K\sqrt{\rho} \tag{2}$$

Investigating the data presented in Fig. 4a, it can be seen that the yield strength of the TW samples is almost 2.6 times higher than that of the AA samples at 20 °C due to the microstructural changes introduced by the two-step thermo-mechanical process (Figs. 1 and 2). More importantly, this yield strength ratio climbs to above 4.2 times as the test temperature increases to 500 °C. Comparing the AA and TW samples at each temperature, α, μ, and b are the same in both cases since they are intrinsic material properties, thus, the strengthening should originate from the increase in the Taylor factor and/or decrease in dislocation

mean free path in the TW samples, according to Eq. (1). The reason for the increase in the yield strength in the TW samples can be further broken down into three potential factors: a shorter effective dislocation mean free path due to the presence of nano-twin boundaries and nano-twin bundles, a higher dislocation density potentially because of not all dislocations being recovered during the recovery heat treatment (1 h at 800 °C) during the two-step processing (Fig. 1), and the changes in the crystallographic texture as a result of 30% deformation at room temperature twice in the TW samples (Fig. 1). These factors can be represented as:

$$\uparrow YS|_{T}^{AA\rightarrow TW} = \Delta(k.d^{-n}) + \Delta\left(\alpha.\mu.b\sqrt{\rho}\right) + \Delta(\overline{M}\tau) \quad (3)$$

where $\uparrow YS|_{T}^{AA\rightarrow TW}$ is the increase in the yield strength at each temperature due to the two-step thermo-mechanical processing as the AA samples turn into the TW samples, $\Delta(k.d^{-n})$ is the Hall-Petch strengthening due the presence of boundaries (grains or twins) as barriers to dislocation motion. In a general Hall-Petch equation, k is the strengthening coefficient and d is the effective grain size, and the exponent n is usually assumed to be 0.5. The term $\Delta(\alpha.\mu.b\sqrt{\rho})$ represents the strengthening due to an increase in dislocation density (ρ) [43]. Next term, $\Delta(\overline{M}\tau)$, indicates the increase in strength due to the crystallographic texture difference, which can be approximated as Taylor factor ($\overline{M}$) times critical resolved shear stress (τ). Eq. (3) should effectively represent the yellow arrows in Fig. 4a. Based on Fig. 4a and Eq. (3), the following arguments can be made:

- Taylor factors in both sample conditions should not change at these relatively low test temperatures (<0.46 homologous temperature T_H) without any prior deformation since changing Taylor factor notable would require substantial change in crystallographic texture, which would require significant plastic deformation level. τ, on the other hand, decreases with increasing temperature,
- Similarly, b doesn't notably change with temperature in this temperature range but μ decreases with temperature, and although no recrystallization occurs below 800 °C in short durations, ρ may decrease with temperature due to recovery in this temperature range.

Therefore, the difference in the dislocation mean free paths of the AA and TW samples should be primarily responsible for the increase in the yield strength ratio as the temperature increases (the first right-hand term in Eq. (3)). The hierarchical twin structure and abundant twin boundaries in the TW samples, introduced via the two-step thermo-mechanical process, should be providing efficient barriers for dislocation motion and help with dislocation storage, even at temperatures as high as 400 °C (0.4 T_H) making 316 austenitic stainless steel more temperature tolerant.

As for UTS, the details of which are provided in Fig. 4b, a general decrease in strength is present as the temperature is increased. Increasing the temperature from 20 °C to 500 °C causes UTS to drop by ~30% for both the AA and TW samples. On average, an increase of 30–35% in UTS is observed as a result of thermally stable deformation twins in the TW samples as compared to the AA samples.

True stress (σ) and true strain (ε) responses from the same tests were plotted and presented in Fig. 3d. For ease of comparison, all AA and TW plots are shown in the same graph, as well as the response of the steel during its second deformation as depicted in Fig. 1. The second deformation curve in the figure belongs to the sample that has already experienced a single cycle of 30% rolling +800 °C for 1 h. Based on the three curves at 20 °C, it can be seen that after each cycle of 30% rolling +800 °C for 1 h treatment, the flow stress increases. The first thermo-mechanical cycle creates an overall ~270 MPa increase in strength. The second thermo-mechanical cycle results in an overall increase of ~160 MPa. At high temperatures, the TW samples exhibits higher maximum true stress levels at necking than their AA counterparts. This observation points out to the benefits of the microstructure created by the thermo-mechanical process. Additionally, the proposed thermo-mechanical process increases the strength of the steel without a total loss of ductility. Even at 500 °C, the sample shows 6% uniform plastic deformation. This is achieved through creating thermally stable deformation twins that impede dislocation glide, while partly recovering the dislocations during heat treatment. Moreover, twin boundaries, based on their type of reactions with the dislocations (emitting sessile/glissile dislocations or glide along the twin boundary) are better in maintaining ductility compared to regular grain boundaries [6,23,44–46].

Another factor that needs to be taking into consideration related to the ductility is the sample size differences. Due to the nature of the process, AA tensile samples have slightly different size than TW samples do. TW samples are thinner and longer, as shown in Fig. 2-a, since they have undergone the thermo-mechanical process. Geometry of tensile samples has an effect on measured ductility according to Ref. [47], in particular the thickness affects the ductility due to geometrical instabilities during necking and fracture modes. The "shorter, thicker specimens tend to be more ductile" [47], possibly contributing to lower observed ductility in TW samples.

The uniform plastic strain (ε_p^u), calculated as true strain up to necking minus the elastic region, is reported in Fig. 4c. It is observed that as the temperature increases, the ε_p^u decreases rapidly at first, then slowly, until it reaches an almost constant value. This decrease is simply because the geometrical instability (necking) occurs sooner at higher temperatures, indicating deterioration in the dislocation storage capacity. Increasing the temperature from 20 °C to 500 °C causes a drop of ~40% and ~60% in ε_p^u for the AA and TW samples, respectively. On average, application of the present thermo-mechanical process causes a decrease of ~70% in the ε_p^u at each temperature. This decrease observed in the TW samples indicates that necking occurs sooner, partly because the stress at the onset of necking is 30–35% higher than that of the AA samples. Despite such a decrease in ε_p^u, the TW samples still exhibit notable uniform plastic deformation after yielding as compared to the conventionally cold-worked 316 austenitic stainless steels, considering the reports that conventionally cold rolled (to 20% thickness reduction) samples neck right after yielding above 100 °C [36]. The results in Ref. [36] demonstrated that the cold-worked samples fail by prompt necking at yield when the yield stress reaches the UTS of the annealed samples. On the other hand, in the present study, the TW samples still displays significant uniform plastic deformation even after their flow stress exceeds the UTS of the AA samples at the same temperature, clearly indicating the influence of the microstructure of the TW samples as compared to those of the conventionally cold worked 316-type austenitic stainless steels. For example, according to engineering stress-strain graph, at 20 °C, the AA sample necks at around 640 MPa, while the TW sample at 20 °C shows almost 17% uniform deformation from 640 MPa to 835 MPa (where it necks). Moreover, at 200 °C for example, the TW sample yields at stress levels well above the UTS of the AA sample at the same temperature.

To complete the above comparative, total hardening rates for each tensile test were calculated as the difference between the yield and ultimate tensile strengths, divided by the uniform plastic strain. The results are presented in Fig. 4d. Based on this graph, the total hardening rates of the AA samples increases from ~1 GPa to ~1.3 GPa as the temperature increases from 20 °C to 500 °C, while the for TW samples, the increase is from ~1.15 GPa to 2.55 GPa. In addition, the differences in total hardening rate at each temperature between the AA and TW samples increase noticeably with temperature: ~0.25 GPa at 20 °C vs. ~1.3 GPa at 500 °C. This trend also points out the effectiveness of this hierarchical, thermally-stable, highly-twinned structure in impeding with deformation mechanisms (mostly dislocation glide) as temperature increases.

The true stress vs. true strain graphs of both the AA and TW samples at 500 °C are presented in Fig. 3e. Their behavior is very similar to that

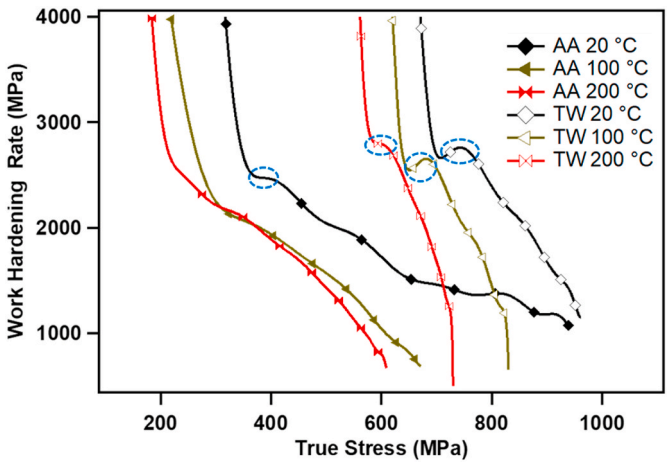

Fig. 5. Work Hardening Rate ($\frac{d\sigma}{d\varepsilon}$) vs. True Stress ($\sigma$) for 316 austenitic stainless steel samples in the AA and TW conditions at temperatures 20 °C, 100 °C, and 200 °C, showing features corresponding to deformation twinning marked by the dashed circles.

of their counterparts at 400 °C. The curves at 500 °C, however, start to show serrations which are known to be due to dynamic strain aging (DSA) [48]. At a closer look, as presented in Fig. 3f and g, it can be seen that the serrations seem to be of different types. For the AA samples, as shown in Fig. 3f, the serrations appear to be Type A, accompanied by Type B, as introduced by Rodriguez [49]. Type A appears as repeated rises followed by drops in the σ-ε curve, which correspond to locking and releasing of dislocations in the deformation bands. Type B appears as oscillations due to the discontinuous motion of dislocations within a deformation band, and usually appear alongside Type A with increasing strain. As for the TW samples in Fig. 3g, the serrations appear less orderly: it is possible to distinguish a pattern of underlying Type A, with the presence of Type B, and even a general trend that may be considered as Type D. Type D serrations appear as increases in strength followed by plateaus that are believed to be similar to Luders band formations. Similar behavior has been reported in tensile behavior of 316 austenitic stainless steels at elevated temperatures, especially when grain size is decreased from 125 μm to 40 μm [49–52]. Since these serrations only appear at higher temperatures, they are unlikely to be due to formation of twins during deformation at such temperatures [53–55]. In the present work, the change in the serration type is not only due to formation of twin bundles with nano-twins (and DSA occurs preferably at boundaries at elevated temperatures [56]), but also the hierarchical structure, that creates general length-scales of two very different magnitudes: one in μms range between bundles and grain boundaries, one in nms range between nano-twin bands. This hypothesis is also likely when considering that DSA occurs due to the pinning of dislocations by solute atoms (C, N, etc.) or vacancies. Depending on whether the domain where the diffusion of these species is occurring is large or small, the rate of their diffusion (and thus the rate of DSA) can change depending on the domain size.

Another finding in this work is related the work hardening rate, defined as the derivative of the true stress over true strain, plotted vs. true stress, and presented in Fig. 5. In all the cases plotted, the initial decrease in the hardening rate due to start of plastic flow is followed by a slower decline, flat or even an increasing trend, which is related to

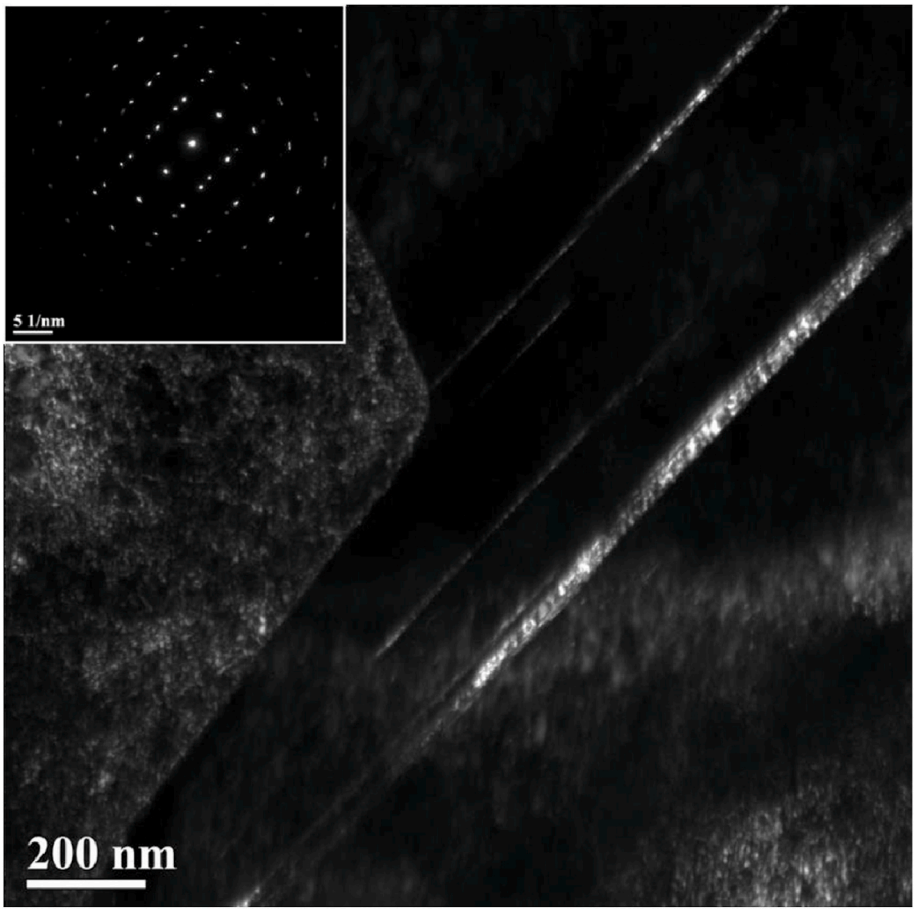

Fig. 6. Dark field TEM image of the AA sample deformed to failure at 100 °C showing deformation twins and the associated SADP as the inset of the image confirming the twinning.

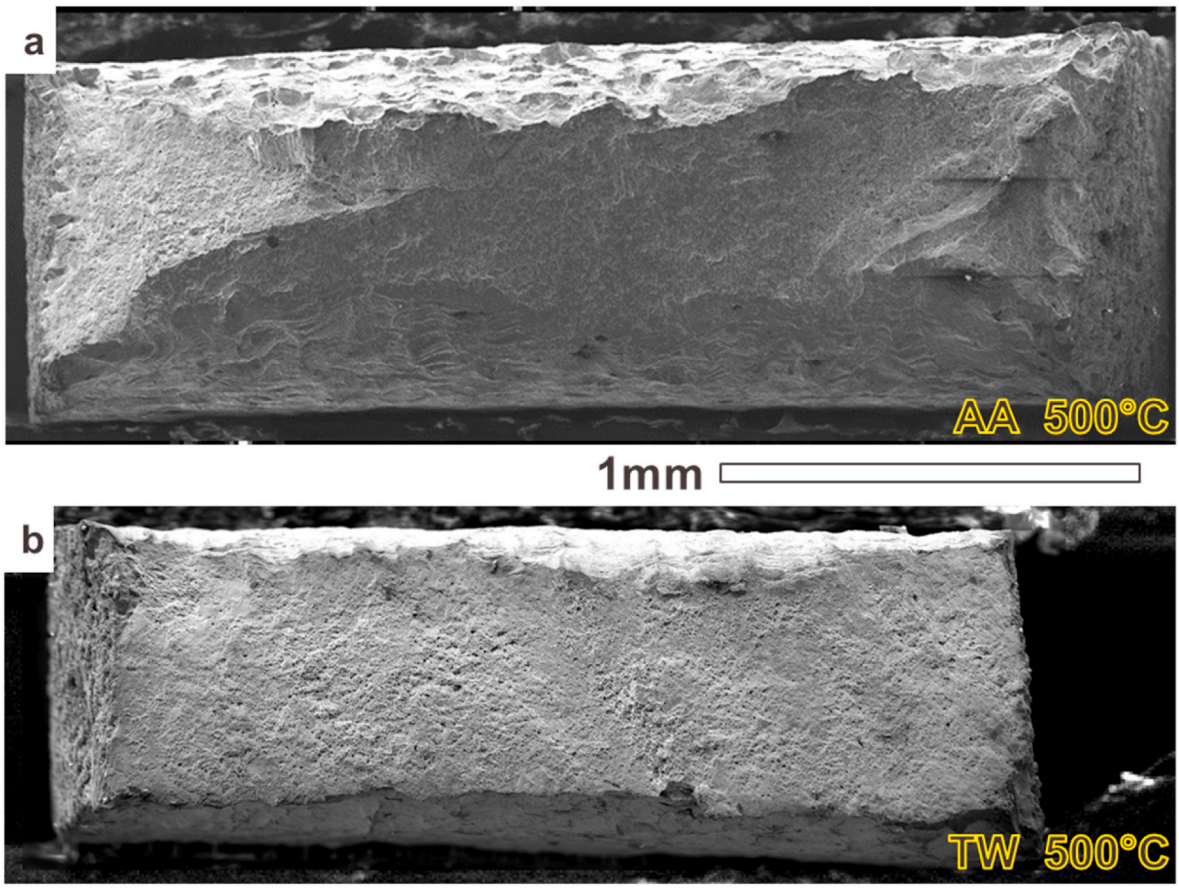

Fig. 7. Fracture surfaces of the samples deformed to failure at 500 °C for a) the AA and b) TW conditions, depicting that the AA samples shows necking and a cup and cone fracture surface, while the TW samples has a flatter fracture surface.

formation of primary twins [38,57]. This trend is witnessed up to 100 °C for the AA samples and up to 200 °C for the TW samples, but not at temperatures 300 °C and above (not shown here), simply because deformation twinning does not occur at higher temperatures. Fig. 6 is a TEM micrograph of an AA sample deformed to failure at 100 °C, and the corresponding selected area diffraction pattern confirming the formation of twins at this temperature. Scanning electron microscopy also shows presence of thin bands on this sample but significantly thinner and sparser (not shown). Such features were not found in the AA samples deformed at 200 °C and above, and therefore, formation of twins at such temperatures cannot be confirmed. For the TW samples shown in Fig. 5, the hardening rate increases over a short range of strain then decreases, indicating the formation of higher volume fraction of deformation twins as compared to the AA samples. This behavior has been witnessed in alloys that are capable of producing a large twinning fraction [58], and occurs at strains above ~ 10%, while in the present case of the TW samples, it occurs at strain levels as small as 2%. It must be added that this behavior in the TW samples is observed at stress levels much higher than those of the AA samples. Clearly, the presence of the thermally-stable twins seems to provide high strength levels that allow

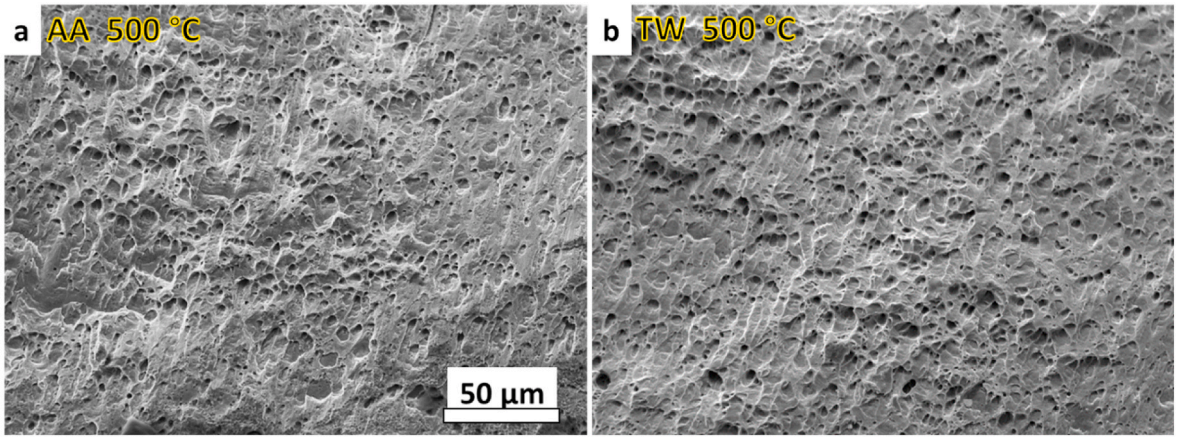

Fig. 8. Higher-magnification images of the fracture surfaces after the deformation to failure at 500 °C for a) the AA and b) TW conditions, showing no significant differences related to the hierarchical thermally-stable twins is observable.

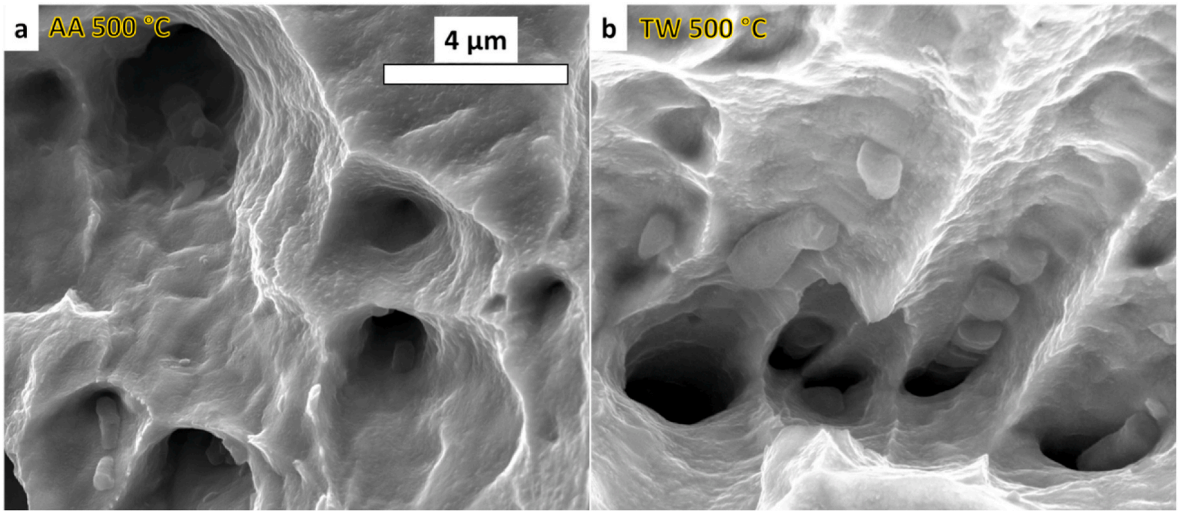

Fig. 9. Close-up images from the dimples on fracture surfaces after the deformation to failure at 500 °C for a) AA and b) TW conditions, showing no significant differences.

additional formation of twins at temperatures as high as 200 °C. Moreover, twins with smaller spacing were found to have more impact in increasing strain hardening rate [26].

Lastly, fracture surfaces of the samples deformed at 500 °C were analyzed for both the AA and TW samples to study the role of thermally-stable deformation twins at high-temperature fracture. At a lower magnification, Fig. 7, the fracture surface of the AA sample shows more necking, and a cup-and-cone style fracture. On the other hand, the fracture surface of the TW sample is flatter, and shows evidence of less necking as compared to the AA sample. Both surfaces, however, displays the features of ductile fracture, which is expected at 500 °C. Upon a closer look at these fracture surface, as depicted in Fig. 8, it is witnessed that in fact not much difference can be detected between the two surfaces. Both the AA and TW samples display dimple fracture surfaces, with the dimples are elongated at different orientations depending on the orientation of each grain. Fig. 9 provides more details from dimples. The dimples for both AA and TW appear to be deep and elongated, and both have particles inside which are impurity particles trapped inside the voids. This is an interesting finding, especially given that the TW samples neck at stress levels ~150 MPa higher than the AA samples. Keep in mind that twin boundaries have been found to be a barrier against void coalescence during fracture, and may be "pulled-out" from a fracture surface [22], similar to a hard particle. These findings, however, suggest that these thermally-stable twins, while playing a role in strengthening the material, do not adversely affect the fracture behavior of a twinned alloy (e.g. do not cause sliding or promote crack propagation even at elevated temperatures).

4. Summary and conclusions

To summarize, in the present work, a two-step thermo-mechanical processing was employed to create a hierarchical microstructure in 316 austenitic stainless steel, consisting of thermally-stable nano-twin bands that form micron-sized bundles with relatively low dislocation density and elongated grains. This structure was tested under uniaxial tension tests at temperatures ranging from 20 °C to 500 °C to reveal the role of pre-existing twin boundaries and twin bundles on the high temperature mechanical response of 316 austenitic stainless steel. The mechanical responses demonstrated a significant improvement in the yield strength levels in the samples with hierarchical twin structures at all temperatures as high as 500 °C due to the shorter mean free path for dislocations. It was concluded that it is the nano-twin boundaries that impart a "thermally tolerant" increase in yield strength. In addition, ultimate tensile strengths of the alloy increase, particularly without a total loss in ductility even at flow stresses above the plastic instability stress of the annealed steel. Stress-strain curves at 500 °C display serrations in the stress-strain response which follows the expected serration mechanisms in the annealed alloy but they are irregular in the twinned alloy. The irregularities were proposed to be a consequence of the hierarchical microstructure and the two different length-scales that they create. The work hardening rate vs. true stress curves indicate that twinning can further occur at elevated temperatures, more so in the initially twinned samples as compared to the annealed samples. The high-temperature fracture surfaces of both conditions were studied and the presence of twins were found to have no adverse effect on failure mechanism.

The hierarchical microstructure with thermally-stable deformation twins demonstrate promise for applications which require high strength. Creating such a structure does not require complex or costly methods: only a combination of cold work and heat treatment at a proper temperature, for example, in commercial steel rolling practices. A hierarchical microstructure like this, while already provides strengthening at high-temperature and thermally tolerant due to lower energy levels of twin boundaries compared to regular grain boundaries, can be further stabilized with precipitation hardening. Precipitates should start forming on the twin boundaries and pin these boundaries against deformations even at higher temperatures. It will be of particular interest to study the performance of such an intricate structure under temperatures above homologous temperature in precipitation hardenable austenitic stainless steels.

Data availability statement

The data that support the findings of this study are available from the corresponding author, [IK], upon reasonable request.

CRediT authorship contribution statement

Taymaz Jozaghi: Methodology, Investigation, Writing – original draft, Writing – review & editing, Visualization. **Peyman Samimi:** Investigation, Visualization, Writing – review & editing. **Yuriy Chumlyakov:** Conceptualization, Methodology, Writing – review & editing, Resources. **Ibrahim Karaman:** Conceptualization, Methodology, Writing – review & editing, Validation, Supervision, Funding acquisition, Resources, Project administration.

Declaration of competing interest

The authors declare that they have no known competing financial interests or personal relationships that could have appeared to influence the work reported in this paper.

Acknowledgement

The present research was supported by the Chevron Professorship I at Texas A&M University. This study was supported by the Tomsk State University Development Programme («Priority-2030»).

References

[1] R. Viswanathan, W. Bakker, Materials for ultrasupercritical coal power plants—boiler materials: Part 1, J. Mater. Eng. Perform. 10 (1) (2001) 81–95.
[2] R. Viswanathan, W. Bakker, Materials for ultrasupercritical coal power plants—turbine materials: Part II, J. Mater. Eng. Perform. 10 (1) (2001) 96–101.
[3] T. Sourmail, Precipitation in creep resistant austenitic stainless steels, Mater. Sci. Technol. 17 (1) (2001) 1–14.
[4] M. Taneike, F. Abe, K. Sawada, Creep-strengthening of steel at high temperatures using nano-sized carbonitride dispersions, Nature 424 (6946) (2003) 294–296.
[5] Y. Yamamoto, M.P. Brady, Z.P. Lu, P.J. Maziasz, C.T. Liu, B.A. Pint, K.L. More, H. Meyer, E.A. Payzant, Creep-resistant, Al2O3-forming austenitic stainless steels, Science 316 (5823) (2007) 433–436.
[6] I. Karaman, H. Sehitoglu, A. Beaudoin, Y. Chumlyakov, H. Maier, C. Tome, Modeling the deformation behavior of Hadfield steel single and polycrystals due to twinning and slip, Acta Mater. 48 (9) (2000) 2031–2047.
[7] I. Karaman, H. Sehitoglu, H. Maier, Y. Chumlyakov, Competing mechanisms and modeling of deformation in austenitic stainless steel single crystals with and without nitrogen, Acta Mater. 49 (19) (2001) 3919–3933.
[8] Z. You, X. Li, L. Gui, Q. Lu, T. Zhu, H. Gao, L. Lu, Plastic anisotropy and associated deformation mechanisms in nanotwinned metals, Acta Mater. 61 (1) (2013) 217–227.
[9] S. Ni, Y. Wang, X. Liao, R. Figueiredo, H. Li, S. Ringer, T. Langdon, Y. Zhu, The effect of dislocation density on the interactions between dislocations and twin boundaries in nanocrystalline materials, Acta Mater. 60 (6–7) (2012) 3181–3189.
[10] Y. Cao, Y. Wang, X. An, X. Liao, M. Kawasaki, S. Ringer, T. Langdon, Y. Zhu, Grain boundary formation by remnant dislocations from the de-twinning of thin nano-twins, Scripta Mater. 100 (2015) 98–101.
[11] J.W. Christian, S. Mahajan, Deformation twinning, Prog. Mater. Sci. 39 (1) (1995) 1–157.
[12] A.T. Krawczynska, S. Gierlotka, P. Suchecki, D. Setman, B. Adamczyk-Cieslak, M. Lewandowska, M. Zehetbauer, Recrystallization and grain growth of a nano/ultrafine structured austenitic stainless steel during annealing under high hydrostatic pressure, J. Mater. Sci. 53 (16) (2018) 11823–11836.
[13] E. El-Danaf, S.R. Kalidindi, R.D. Doherty, Influence of grain size and stacking-fault energy on deformation twinning in fcc metals, Metall. Mater. Trans. 30 (5) (1999) 1223–1233.
[14] I. Karaman, H. Sehitoglu, Y. Chumlyakov, H. Maier, The deformation of low-stacking-fault-energy austenitic steels, J. Occup. Med. 54 (7) (2002) 31–37.
[15] S. Vercammen, B. Blanpain, B. De Cooman, P. Wollants, Cold rolling behaviour of an austenitic Fe–30Mn–3Al–3Si TWIP-steel: the importance of deformation twinning, Acta Mater. 52 (7) (2004) 2005–2012.
[16] G.M. De Bellefon, J. Van Duysen, K. Sridharan, Composition-dependence of stacking fault energy in austenitic stainless steels through linear regression with random intercepts, J. Nucl. Mater. 492 (2017) 227–230.
[17] R. Schramm, R. Reed, Stacking fault energies of seven commercial austenitic stainless steels, Metall. Trans. A 6 (7) (1975) 1345–1351.
[18] S. Yang, J. Spruiell, Cold-worked state and annealing behaviour of austenitic stainless steel, J. Mater. Sci. 17 (3) (1982) 677–690.
[19] Y. Petrov, Surface structure of different interstitial austenitic steels after impact wear, Int. J. Mater. Res. 103 (5) (2012) 551–553.
[20] M. Ojima, Y. Adachi, Y. Tomota, Y. Katada, Y. Kaneko, K. Kuroda, H. Saka, Weak beam TEM study on stacking fault energy of high nitrogen steels, Steel Res. Int. 80 (7) (2009) 477–481.
[21] R.L. Peng, M. Odén, Y. Wang, S. Johansson, Intergranular strains and plastic deformation of an austenitic stainless steel, Mater. Sci. Eng. 334 (1) (2002) 215–222.
[22] L. Xiong, Z. You, S. Qu, L. Lu, Fracture behavior of heterogeneous nanostructured 316L austenitic stainless steel with nanotwin bundles, Acta Mater. 150 (2018) 130–138.
[23] K. Lu, L. Lu, S. Suresh, Strengthening materials by engineering coherent internal boundaries at the nanoscale, Science 324 (5925) (2009) 349–352.
[24] O. Bouaziz, D. Barbier, Benefits of recovery and partial recrystallization of nano-twinned austenitic steels, Adv. Eng. Mater. 15 (10) (2013) 976–979.
[25] Y. Zhao, J. Bingert, X. Liao, B. Cui, K. Han, A. Sergueeva, A. Mukherjee, R. Valiev, T. Langdon, Y. Zhu, Simultaneously elevating the stregth and ductility of ultra-fine-grained pure copper, Adv. Mater. 18 (22) (2006) 2949–2953.
[26] Y. Zhu, X. Liao, X. Wu, Deformation twinning in nanocrystalline materials, Prog. Mater. Sci. 57 (1) (2012) 1–62.
[27] O. Bouaziz, D. Barbier, Strain-hardening in nano-structured single phase steels: mechanisms and control, J. Nanosci. Nanotechnol. 12 (11) (2012) 8732–8734.
[28] J.S. Li, W.D. Gao, Y. Cao, Z.W. Huang, B. Gao, Q.Z. Mao, Y.S. Li, Microstructures and mechanical properties of a gradient nanostructured 316L stainless steel processed by rotationally accelerated shot peening, Adv. Eng. Mater. (2018) 1800402.
[29] J. Li, B. Gao, Z. Huang, H. Zhou, Q. Mao, Y. Li, Design for strength-ductility synergy of 316L stainless steel with heterogeneous lamella structure through medium cold rolling and annealing, Vacuum (2018).
[30] O. Anderoglu, A. Misra, H. Wang, X. Zhang, Thermal stability of sputtered Cu films with nanoscale growth twins, J. Appl. Phys. 103 (9) (2008), 094322.
[31] M. El-Tahawy, Y. Huang, H. Choi, H. Choe, J.L. Lábár, T.G. Langdon, J. Gubicza, High temperature thermal stability of nanocrystalline 316L stainless steel processed by high-pressure torsion, Mater. Sci. Eng. 682 (2017) 323–331.
[32] X. Wang, H. Zurob, J. Embury, X. Ren, I. Yakubtsov, Microstructural features controlling the deformation and recrystallization behaviour Fe–30% Mn and Fe–30% Mn–0.5% C, Mater. Sci. Eng. 527 (16) (2010) 3785–3791.
[33] O. Bouaziz, C. Scott, G. Petitgand, Nanostructured steel with high work-hardening by the exploitation of the thermal stability of mechanically induced twins, Scripta Mater. 60 (8) (2009) 714–716.
[34] D. Fabrègue, O. Bouaziz, D. Barbier, Nano-twinned steel exhibits high mechanical properties obtained through ultra-rapid heat treatment, Mater. Sci. Eng. 712 (2018) 765–771.
[35] X. Zhang, A. Misra, Superior thermal stability of coherent twin boundaries in nanotwinned metals, Scripta Mater. 66 (11) (2012) 860–865.
[36] T. Byun, N. Hashimoto, K. Farrell, Temperature dependence of strain hardening and plastic instability behaviors in austenitic stainless steels, Acta Mater. 52 (13) (2004) 3889–3899.
[37] B. Zhang, F. Yan, M. Zhao, N. Tao, K. Lu, Combined strengthening from nanotwins and nanoprecipitates in an iron-based superalloy, Acta Mater. 151 (2018) 310–320.
[38] S. Wang, T. Jozaghi, I. Karaman, R. Arroyave, Y. Chumlyakov, Hierarchical evolution and thermal stability of microstructure with deformation twins in 316 stainless steel, Mater. Sci. Eng. 694 (2017) 121–131.
[39] G.I. Taylor, The mechanism of plastic deformation of crystals. Part I.—Theoretical, Proc. R. Soc. Lond. - Ser. A Contain. Pap. a Math. Phys. Character 145 (855) (1934) 362–387.
[40] K.M. Davoudi, J.J. Vlassak, Dislocation evolution during plastic deformation: equations vs. discrete dislocation dynamics study, J. Appl. Phys. 123 (8) (2018), 085302.
[41] S. Mishra, M. Yadava, K.N. Kulkarni, N. Gurao, A new phenomenological approach for modeling strain hardening behavior of face centered cubic materials, Acta Mater. 178 (2019) 99–113.
[42] O. Bouaziz, N. Guelton, Modelling of TWIP effect on work-hardening, Mater. Sci. Eng. 319 (2001) 246–249.
[43] T. Narutani, J. Takamura, Grain-size strengthening in terms of dislocation density measured by resistivity, Acta Metall. Mater. 39 (8) (1991) 2037–2049.
[44] T. Zhu, J. Li, A. Samanta, H.G. Kim, S. Suresh, Interfacial plasticity governs strain rate sensitivity and ductility in nanostructured metals, Proc. Natl. Acad. Sci. Unit. States Am. 104 (9) (2007) 3031–3036.
[45] I. Karaman, H. Sehitoglu, K. Gall, Y. Chumlyakov, H. Maier, Deformation of single crystal Hadfield steel by twinning and slip, Acta Mater. 48 (6) (2000) 1345–1359.
[46] Z.-H. Jin, P. Gumbsch, K. Albe, E. Ma, K. Lu, H. Gleiter, H. Hahn, Interactions between non-screw lattice dislocations and coherent twin boundaries in face-centered cubic metals, Acta Mater. 56 (5) (2008) 1126–1135.
[47] Y. Zhao, Y. Guo, Q. Wei, A. Dangelewicz, C. Xu, Y. Zhu, T. Langdon, Y. Zhou, E. Lavernia, Influence of specimen dimensions on the tensile behavior of ultrafine-grained Cu, Scripta Mater. 59 (6) (2008) 627–630.
[48] A. Van den Beukel, Theory of the effect of dynamic strain aging on mechanical properties, Phys. Status Solidi 30 (1) (1975) 197–206.
[49] P. Rodriguez, Serrated plastic flow, Bull. Mater. Sci. 6 (4) (1984) 653–663.
[50] S. Mannan, K. Samuel, P. Rodriguez, Dynamic strain aging in type 316 stainless steel, Trans. Indian Inst. Met. 36 (4) (1983) 313–320.
[51] S. Mannan, K. Samuel, P. Rodriguez, The influence of grain size on elevated temperature deformation behaviour of a type 316 stainless steel, in: Strength of Metals and Alloys (ICSMA 6), Elsevier, 1982, pp. 637–642.
[52] S. Mannan, K. Samuel, P. Rodriguez, Stress-strain relation for 316 stainless steel at 300K, Scripta Metall. 16 (3) (1982) 255–257.
[53] G. Bolling, R. Richman, Continual mechanical twinning: Part III: nucleation and dislocation production Part IV: cyclic twinning in Fe3Be single crystals, Acta Metall. 13 (7) (1965) 745–757.
[54] G. Bolling, R. Richman, Continual mechanical twinning: Part II: standard experiments, Acta Metall. 13 (7) (1965) 723–743.
[55] G. Bolling, R. Richman, Continual mechanical twinning: part I: formal description, Acta Metall. 13 (7) (1965) 709–722.
[56] R. Armstrong, in: A.R. ROSENFIELD, G.T. HAHN, A.L. BEMENT Jr. (Eds.), Dislocation Dynamics, RI JAFFEE, 1968, p. 293.
[57] B.C. De Cooman, Y. Estrin, S.K. Kim, Twinning-induced plasticity (TWIP) steels, Acta Mater. 142 (2018) 283–362.
[58] J. Kim, Y. Estrin, H. Beladi, I. Timokhina, K.-G. Chin, S.-K. Kim, B.C. De Cooman, Constitutive modeling of the tensile behavior of Al-TWIP steel, Metall. Mater. Trans. 43 (2) (2012) 479–490.